Biophysical *Journal*
Biophysical Letter

Biophysical Society

Increased Tissue Stiffness in Tumors from Mice with Neurofibromatosis-1 Optic Glioma

Christopher Walter,[1] Lindsey Crawford,[2] Melinda Lai,[3] Joseph A. Toonen,[2] Yuan Pan,[2] Shelly Sakiyama-Elbert,[4] David H. Gutmann,[2] and Amit Pathak[1,3,*]

[1]Department of Biomedical Engineering, Washington University, St. Louis, Missouri; [2]Department of Neurology, Washington University School of Medicine, St. Louis, Missouri; [3]Department of Mechanical Engineering and Materials Science, Washington University, St. Louis, Missouri; and [4]Department of Biomedical Engineering, University of Texas-Austin, Austin, Texas

ABSTRACT Children with neurofibromatosis type 1 (NF1) cancer predisposition syndrome are prone to the development of low-grade brain tumors (gliomas) within the optic pathway (optic gliomas). One of the key obstacles to developing successful therapeutic strategies for these tumors is the striking lack of information about the mechanical properties that characterize these tumors relative to non-neoplastic optic nerve tissue. To study the physical changes that may occur when an optic nerve glioma is present, we employed atomic force microscopy to measure the stiffness of healthy versus tumor-bearing optic nerve tissue. We found that the average elastic moduli of non-neoplastic and tumor-bearing optic nerves were ~3 and ~6 kPa, respectively. Based on previous studies implicating changes in extracellular matrix remodeling in other, related optic nerve pathological states, we found decreased expression of one major metalloproteinase protein (MMP-2) and unchanged expression of lysyl oxidase and a second metalloproteinase, MMP-9, in murine optic gliomas relative to normal non-neoplastic optic nerve. Collectively, these observations suggest a productive interplay between physical properties of mouse optic nerve gliomas and the extracellular matrix.

Brain tumors represent the most common solid tumor in children, with low-grade gliomas (LGGs) accounting for the majority of these neoplasms (1–3). Among these LGGs, many arise within the optic pathway (optic pathway gliomas (OPGs)). Although most of these OPGs arise in the absence of a predisposing genetic syndrome, the presence of an OPG should raise suspicion for neurofibromatosis type 1 (NF1), a nervous system cancer predisposition syndrome that causes tumors in the optic pathway (4–6). Of the population of children affected by NF1 syndrome, 15–20% of affected children will develop an OPG.

With the identification of the *Nf1* gene, it became possible to develop small-animal models of NF1-associated OPG (7). The generation of these strains represented a critical first step toward the identification of efficacious treatments for these tumors, as NF1-OPGs are rarely resected and renewable human biological specimens are not available. In this regard, numerous molecular targets have been discovered using these *Nf1* genetically engineered mouse (GEM) models, several of which have been evaluated as potential chemotherapies in children with NF1-OPG (8–10).

However, NF1-OPGs, similar to their sporadic pilocytic astrocytoma counterparts, are complex ecosystems composed of both cellular and acellular components. Analysis of human LGGs, including rare NF1 pilocytic astrocytomas, has demonstrated that 30–50% of the cells in these tumors are immune-system-like cells (macrophages and microglia) embedded within a rich extracellular matrix (11,12). Although intense study of the role of macrophages and microglia has revealed additional targets for stroma-directed therapies, the contribution of the extracellular matrix (ECM) remains unexplored.

In many types of cancer, including breast, brain, and colorectal cancers (13–15), cell growth and ECM remodeling that occur during tumor development alter the mechanical properties of the tumor. As such, breast and colorectal tumors have been found to be stiffer than their surrounding healthy tissue (13,15). Lymph nodes also have been found to increase in stiffness when invaded by metastatic lung carcinoma cells (14). This rise in stiffness is also associated with enhanced metastatic potential of cancer cells (16,17). Although such relationships, i.e., between tumor development and stiffness, have been established for a variety of

Submitted December 5, 2016, and accepted for publication March 23, 2017.

*Correspondence: pathaka@wustl.edu

Christopher Walter and Lindsey Crawford contributed equally to this work.

Editor: Philip LeDuc.

http://dx.doi.org/10.1016/j.bpj.2017.03.017

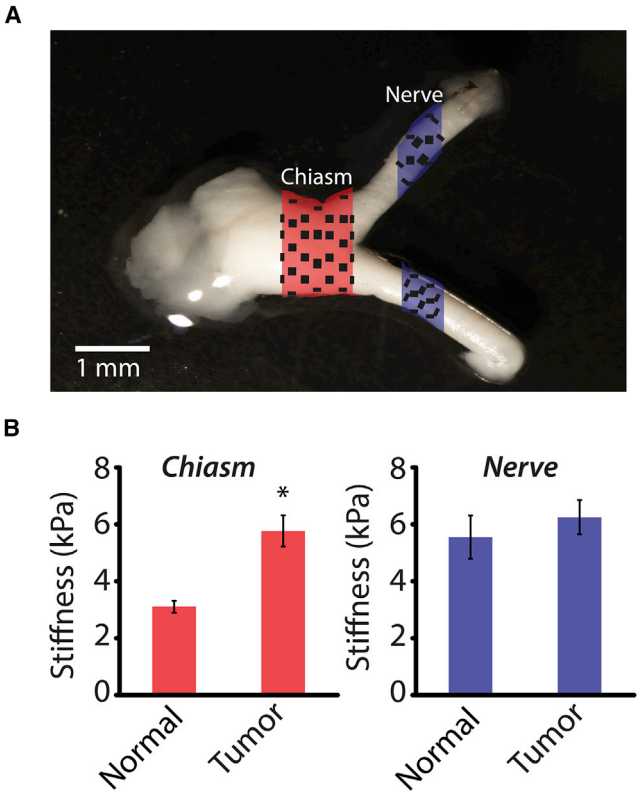

FIGURE 1 Increased stiffness of glioma-bearing optic nerves at the chiasm. (*A*) Diagram describing the two regions where AFM measurements were taken, the chiasm and the optic nerve (≥1 mm proximal to the chiasm). (*B*) Average tissue stiffness obtained using AFM. Error bars represent the mean ± SE. $N > 34$; *$p < 0.05$. To see this figure in color, go online.

cancer types, the mechanical properties of optic nerve glioma, as well as their underlying acellular causes, are unknown.

The normal optic nerve is a complex tissue composed of numerous distinct cellular and extracellular components. Similarly, optic nerve gliomas harbor a unique collection of neoplastic (astrocytes and stem cells) and non-neoplastic (endothelial cells and microglia) cell types embedded within a rich ECM. In this manner, the normal and neoplastic optic nerve tissues represent distinct ecological systems. As such, future therapies might leverage the physical properties unique to the optic glioma ecosystem as a means of targeting the specialized determinants of the tumor. This information is critical to the design of future in vitro platforms to perform drug-screening studies for these optic nerve tumors.

To examine the ECM and mechanical properties associated with murine *Nf1* optic glioma, we employed atomic force microscopy (AFM), which allows for mechanical testing of small tissues in defined areas. In this study, we found that, similar to other LGGs, *Nf1* optic glioma tissues are stiffer than healthy tissue. To establish a relationship between the ECM and mechanical properties, we also evaluated the levels of matrix metalloproteases (MMP-2 and MMP-9), which are important for ECM degradation (18), and lysyl oxidase (LOX), which is associated with ECM cross-linking (19). Consistent with the mechanical properties of our optic glioma system, we also found differing expression of MMP-2 in glioma-bearing optic nerves relative to controls.

Increased stiffness of tumor-bearing optic nerves

Optic nerves were harvested from 3-month-old mice at a time when optic gliomas are obvious (20), and covalently attached to glass slides precoated with poly-L-lysine. OPGs in children with NF1 typically arise in the prechiasmatic optic nerves and chiasm, similar to those arising in *Nf1* mutant mice. Using AFM, the elastic modulus of the optic nerves was tested in two sections, at the chiasm and in unaffected portions of the optic nerve (≥2 mm proximal to the chiasm). Briefly, in AFM, piezoelectric actuators are used to control the x, y, and z positions of a cantilever probe, which is indented into the surface of a given tissue sample (Fig. S1). The cantilever deflection is used to calculate the indentation force of the probe and these force-deflection data are translated into the elastic modulus of the sample using a model, typically the Hertz model (21,22). The nerves were tested at various points across the width, and the measurements were averaged (Fig. 1 *A*). At the chiasm, the glioma-bearing nerves were significantly stiffer than their normal (non-neoplastic) counterparts, 5.8 ± 0.5 kPa and 3.1 ± 0.6 kPa, respectively, an 85% increase (Fig. 1 *B*). In contrast, the stiffness of the unaffected optic nerve segments in the wild-type (6.9 ± 1.4 kPa) was similar to that in glioma-bearing nerves (6.6 ± 0.8 kPa). These findings indicate that the mechanical consequences of tumor development in the *Nf1* mutant mice remain localized in the chiasm region and do not propagate into distant areas of the optic nerve tissue. These tumor-related mechanical changes in the optic nerve, along with the knowledge that NF1 tumors are characterized by ECM changes (23), could indicate that regulation of matrix-modifying proteins is a key factor in the development of these tumors.

ECM-modifying enzyme expression is altered in glioma-bearing optic nerves

One of the hallmarks of solid tumors is the production of enzymes that modify ECM components, including MMPs (18). To examine the expression of these enzymes in the murine *Nf1* optic glioma model, immunohistochemistry (IHC) was performed in 3-month-old mice with *Nf1* optic glioma and in wild-type control mice using antibodies against MMP-2, MMP-9, and LOX (Figs. 2, S2, and S3, respectively). Given the localization of the glioma mainly to the chiasm and the results of the AFM experiments, the protein levels at the chiasm were compared to those in the unaffected proximal optic nerve segment. Although the intensity of the immmunostaining appears greater in glioma-bearing relative to healthy optic nerves, there was a significant

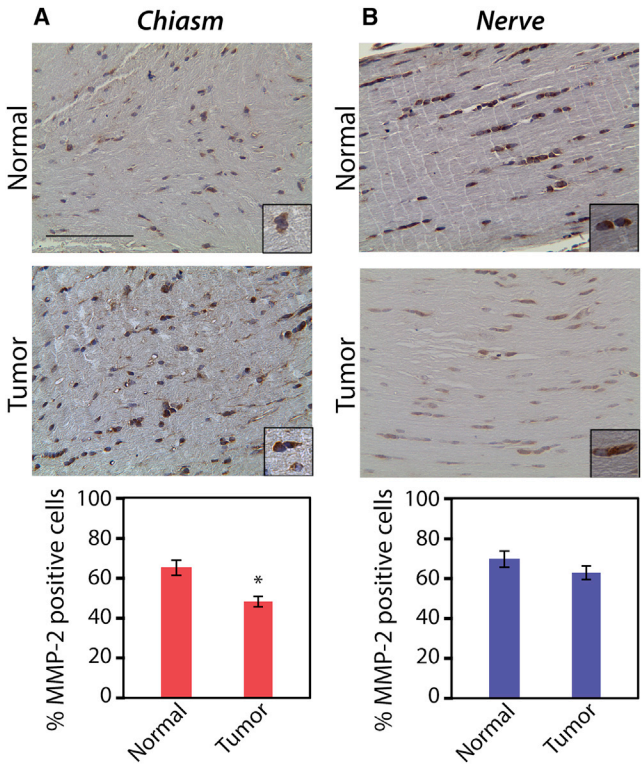

FIGURE 2 Glioma-bearing optic nerves have decreased MMP-2 expression in the chiasm (*A*), but not in the unaffected proximal optic nerve segment (*B*), mirroring the effects shown with AFM. *$p < 0.01$. Error bars represent the mean ± SE. Scale bars represent 100 μm. To see this figure in color, go online.

decrease in the percent of MMP-2-positive cells at the chiasm in the glioma-bearing mice compared to their control counterparts (47.8 ± 1.9% and 64.1 ± 2.4%, respectively). However, in the unaffected proximal optic nerve segment of mice with *Nf1* optic glioma, as compared to controls, there were no differences in MMP-2-positive cells (63.7 ± 5.0% and 68.2 ± 2.7%, respectively). There was also no difference between glioma-bearing and wild-type mice in the percent of LOX-positive cells at the chiasm (42.4 ± 7.6% and 43.3 ± 8.6%, respectively) or in the unaffected proximal optic nerve segment (50.8 ± 2.7% and 56.5 ± 5.3%, respectively). In addition, there was no difference in the percent of MMP-9-positive cells at the chiasm (48.8 ± 5.9% and 37.7 ± 3.5%) or in the unaffected proximal optic nerve segment (46.2 ± 7.5% and 39.4 ± 2.0%).

Thus, complementary to the AFM data, we found decreased MMP-2 protein levels in the chiasms of glioma-bearing optic nerves relative to their wild-type counterparts. MMPs break down fibrous ECM structures, like collagen, to create reorganization within the tumor, and they lead to changes in physical properties. Traditionally, increases in MMP expression and LOX expression are associated with high-grade tumors (24,25). However, in the context of optic nerve glioma, we saw a decrease in MMP-2 and no change in LOX, which suggests less breakdown of collagen fibers (a greater degree of collagen cross-linking). This result is consistent with the stiffer matrix observed by AFM at the chiasm in optic nerves from *Nf1* mutant mice. Although metastatic high-grade gliomas exhibit increases in MMP-2, MMP-9, and LOX, we do not expect to see the same trends in optic nerve glioma, given that they are low-grade tumors and not metastatic cancers (26). Importantly, in the unaffected proximal optic nerve segment, there was no variation in matrix stiffness between neoplastic and non-neoplastic optic nerves. IHC images from this same location also show no significant differences in MMP-2 levels, further supporting the link between decreased MMP-2 protein levels and increased stiffness at the chiasm. In addition, this decrease in MMP-2 expression likely results from loss of *Nf1* gene expression in the neoplastic astrocytes, since *Nf1*-deficient astrocytes exhibit a 40% decrease in *Mmp2* RNA levels relative to their wild-type counterparts, as determined by quantitative reverse transcriptase-polymerase chain reaction (Fig. S4; $p = 0.033$).

Taken together, the results leveraging both AFM and IHC show, to our knowledge, a novel relationship between the metalloproteinase protein levels present in the acellular environment and the physical properties of *Nf1* optic glioma. This work warrants further studies using three-dimensional in vitro platforms to establish mechanistic connections between these acellular and physical properties and optic glioma biology.

SUPPORTING MATERIAL

Supporting Materials and Methods and four figures are available at http://www.biophysj.org/biophysj/supplemental/S0006-3495(17)30336-3.

AUTHOR CONTRIBUTIONS

A.P., D.H.G., and S.S.-E. designed research. C.W., L.C., M.L., J.A.T., and Y.P. performed research, contributed analytic tools, and analyzed data. C.W., L.C., D.H.G., and A.P. wrote the article.

ACKNOWLEDGMENTS

The authors thank Courtney Corman for technical assistance with the quantitative reverse transcriptase-polymerase chain reaction experiments.

This work was in part supported by grants from the National Science Foundation (CAREER Award 1454016 to A.P.), the Edward Mallinckrodt, Jr. Foundation (New Investigator Award to A.P.), the National Cancer Institute (CA195692-01 to D.H.G.), and the National Institutes of Health (T32 Interdisciplinary Training in Mechanobiology to C.W.). D.H.G. acknowledges support from The Giorgio Foundation and a National Institute of Neurological Disorders and Stroke Research Program Award (1-R35-NS097211-01).

REFERENCES

1. Dolecek, T. A., J. M. Propp, …, C. Kruchko. 2012. CBTRUS statistical report: primary brain and central nervous system tumors

diagnosed in the United States in 2005-2009. *Neuro-oncol.* 14 (*Suppl. 5*):v1–v49.

2. Gurney, J. G., D. A. Wall, …, F. G. Davis. 1999. The contribution of nonmalignant tumors to CNS tumor incidence rates among children in the United States. *Cancer Causes Control.* 10:101–105.
3. Louis, D. N., H. Ohgaki, …, P. Kleihues. 2007. The 2007 WHO classification of tumours of the central nervous system. *Acta Neuropathol.* 114:97–109.
4. Listernick, R., D. N. Louis, …, D. H. Gutmann. 1997. Optic pathway gliomas in children with neurofibromatosis 1: consensus statement from the NF1 optic pathway glioma task force. *Ann. Neurol.* 41:143–149.
5. Listernick, R., R. E. Ferner, …, D. H. Gutmann. 2007. Optic pathway gliomas in neurofibromatosis-1: controversies and recommendations. *Ann. Neurol.* 61:189–198.
6. King, A., R. Listernick, …, D. H. Gutmann. 2003. Optic pathway gliomas in neurofibromatosis type 1: the effect of presenting symptoms on outcome. *Am. J. Med. Genet. A.* 122A:95–99.
7. Bajenaru, M. L., M. R. Hernandez, …, D. H. Gutmann. 2003. Optic nerve glioma in mice requires astrocyte *Nf1* gene inactivation and *Nf1* brain heterozygosity. *Cancer Res.* 63:8573–8577.
8. Dasgupta, B., Y. Yi, …, D. H. Gutmann. 2005. Proteomic analysis reveals hyperactivation of the mammalian target of rapamycin pathway in neurofibromatosis 1-associated human and mouse brain tumors. *Cancer Res.* 65:2755–2760.
9. Hegedus, B., D. Banerjee, …, D. H. Gutmann. 2008. Preclinical cancer therapy in a mouse model of neurofibromatosis-1 optic glioma. *Cancer Res.* 68:1520–1528.
10. Arun, D., and D. H. Gutmann. 2004. Recent advances in neurofibromatosis type 1. *Curr. Opin. Neurol.* 17:101–105.
11. Rickman, D. S., M. P. Bobek, …, S. M. Hanash. 2001. Distinctive molecular profiles of high-grade and low-grade gliomas based on oligonucleotide microarray analysis. *Cancer Res.* 61:6885–6891.
12. Sharma, M. K., M. A. Watson, …, D. H. Gutmann. 2006. Matrilin-2 expression distinguishes clinically relevant subsets of pilocytic astrocytoma. *Neurology.* 66:127–130.
13. McKnight, A. L., J. L. Kugel, …, R. L. Ehman. 2002. MR elastography of breast cancer: preliminary results. *AJR Am. J. Roentgenol.* 178:1411–1417.
14. Miyaji, K., A. Furuse, …, S. Omata. 1997. The stiffness of lymph nodes containing lung carcinoma metastases: a new diagnostic parameter measured by a tactile sensor. *Cancer.* 80:1920–1925.
15. Baker, A. M., D. Bird, …, J. T. Erler. 2013. Lysyl oxidase enzymatic function increases stiffness to drive colorectal cancer progression through FAK. *Oncogene.* 32:1863–1868.
16. Swaminathan, V., K. Mythreye, …, R. Superfine. 2011. Mechanical stiffness grades metastatic potential in patient tumor cells and in cancer cell lines. *Cancer Res.* 71:5075–5080.
17. Nasrollahi, S., and A. Pathak. 2016. Topographic confinement of epithelial clusters induces epithelial-to-mesenchymal transition in compliant matrices. *Sci. Rep.* 6:18831.
18. Shay, G., C. C. Lynch, and B. Fingleton. 2015. Moving targets: emerging roles for MMPs in cancer progression and metastasis. *Matrix Biol.* 44-46:200–206.
19. Kise, K., Y. Kinugasa-Katayama, and N. Takakura. 2016. Tumor microenvironment for cancer stem cells. *Adv. Drug Deliv. Rev.* 99 (Pt. B):197–205.
20. Toonen, J. A., Y. Ma, and D. H. Gutmann. 2016. Defining the temporal course of murine neurofibromatosis-1 optic gliomagenesis reveals a therapeutic window to attenuate retinal dysfunction. *Neuro Oncol.* http://dx.doi.org/10.1093/neuonc/now267.
21. Lekka, M., and P. Laidler. 2009. Applicability of AFM in cancer detection. *Nat. Nanotechnol.* 4:72. author reply 72–73.
22. Faria, E. C., N. Ma, …, R. D. Snook. 2008. Measurement of elastic properties of prostate cancer cells using AFM. *Analyst (Lond.).* 133:1498–1500.
23. Daginakatte, G. C., and D. H. Gutmann. 2007. Neurofibromatosis-1 (*Nf1*) heterozygous brain microglia elaborate paracrine factors that promote *Nf1*-deficient astrocyte and glioma growth. *Hum. Mol. Genet.* 16:1098–1112.
24. da Silva, R., M. Uno, …, S. M. Oba-Shinjo. 2015. LOX expression and functional analysis in astrocytomas and impact of IDH1 mutation. *PLoS One.* 10:e0119781.
25. Charles, N. A., E. C. Holland, …, H. Kettenmann. 2011. The brain tumor microenvironment. *Glia.* 59:1169–1180.
26. Wang, M., T. Wang, …, A. Teramoto. 2003. The expression of matrix metalloproteinase-2 and -9 in human gliomas of different pathological grades. *Brain Tumor Pathol.* 20:65–72.

Biophysical Journal, Volume *112*

Supplemental Information

Increased Tissue Stiffness in Tumors from Mice with Neurofibromatosis-1 Optic Glioma

Christopher Walter, Lindsey Crawford, Melinda Lai, Joseph A. Toonen, Yuan Pan, Shelly Sakiyama-Elbert, David H. Gutmann, and Amit Pathak

Supporting Material

for

"Increased Tissue Stiffness in Tumors From Mice with Neurofibromatosis-1 Optic Glioma"

Materials and Methods

Mice and optic nerve dissection

Optic glioma-bearing (*Nf1*$^{flox/mut}$; GFAP-Cre) and WT (either *Nf1*$^{flox/flox}$ or C57BL/6) mice were bred and maintained at Washington University in accordance with an approved Animal Studies Protocol. For all experiments, 3-month-old mice were transcardially perfused with Ringer's solution, based on previous experiments demonstrating that gliomas are evident by this age (1). For AFM applications, optic nerves and chiasms were microdissected and placed in artificial cerebrospinal fluid (aCSF) until analyses were performed. For immunohistochemistry applications, mice were additionally perfused with 4% paraformaldehyde in 0.1 M sodium phosphate buffer (pH 7.4). Optic nerves and chiasms were microdissected and post-fixed in 4% paraformaldehyde. Samples were then embedded in paraffin and sectioned. For all glioma-bearing optic nerve experiments, optic nerves were observed under the microscope to confirm the presence of a glioma involving the chiasm.

Atomic Force Microscopy

Dissected optic nerves were covalently attached to glass slides treated with Poly-L-Lysine (Sigma-Aldrich, St. Louis). Slides were pre-treated for at least 2 hours before attaching the optic

nerves. After attachment, optic nerves were kept in aCSF for the remainder of the experiment. All measurements were acquired using an MFP-3D-BIO atomic force microscope (Asylum Research, Santa Barbara, CA). In AFM, piezoelectric actuators are used to control the x, y, and z position of a probe, consisting of a flexible cantilever with a micron-sized tip attached to a chip. When the probe is near a surface, attractive and repulsive forces between the tip and the sample cause deflection of the cantilever, which is tracked by a laser reflected off the back of the cantilever onto a position-sensitive photodiode detector. To measure the elastic modulus of a sample, the sample (optic nerve surface) is indented by the probe, and the cantilever deflection is measured as a function of the probe's z position. Olympus TR400PB AFM probes with an Au/Cr coated silicon nitride cantilever and pyramidal tip (Asylum Research, Santa Barbara, CA), with reported stiffness of 0.02 N/m, were used to perform AFM on the optic nerves. Tips were initially calibrated in air to determine the spring constant of the cantilever. After determining the cantilever's spring constant, the probes were allowed to equilibrate in aCSF for at least 1 hour in order to prevent drift in the measured deflection due to the aCSF. Probes were then calibrated in aCSF in order to account for residual effects of the fluid during the testing process. To finish the setup procedure, the slides with the optic nerves in aCSF were then placed onto the AFM stage and probes were allowed to equilibrate in the aCSF for 15 min. AFM testing was performed by indenting nerves down the length and across the width of the optic nerves (**Fig. S1**).

To generate a force curve, the cantilever was first lowered close to the surface until a small deflection was measured due to surface interaction with the sample. When the system begins to generate a force curve, the probe approaches the tissue surface until a contact is made. After contact, the tip is indented into the sample until a user-defined threshold indentation force and depth are reached. The tip is then retracted from the sample and returned to its original position. In our measurements, typical force curves were generated by indenting nerves with a force of 10 nN through 2 μm of working distance. Indentation speed was set at 7 μm/s in

order to negate viscous effects of the aCSF. Force curves resembled those of typical viscoelastic materials, with a small contact region following the approach, followed by a linear indentation (**Fig. S1**). The retraction portion of the curve shows sticking behavior, as seen by separation from the indentation curve during the initial portion just past the contact point, where a quick jump is observed, representing the tip "unsticking" from the sample and returning to its original position. Any curves that did not exhibit this behavior were not analyzed.

A modified Hertz model, implemented in MATLAB, was used to analyze the force curves. The Hertz model assumes that the tip does not deform and the tissue sample is linear elastic and of infinite length (2, 3). The modified Hertz model is developed to analyze viscoelastic materials by first normalizing the approach portion of the indentation curve to 0 (4, 5). Then, the model determines the contact point, generates a best-fit curve for maximal overlap with the measured indentation curve, and computes the elastic modulus. This was repeated for 5 samples per condition (wild-type versus glioma-bearing nerves) and the 5 values were averaged.

Immunohistochemistry

Immunohistochemistry was performed on paraffin-embedded optic nerves and chiasms using anti-MMP-9 (1:500 dilution, Abcam ab38898), anti-MMP-2 (1:2000 dilution, Abcam ab110186), and anti-LOX (1:500 dilution, Abcam ab31238) primary antibodies. Antigen retrieval was accomplished in a citrate buffer (pH 6.0) at 100^{o}C for 15 minutes. Primary antibody detection was performed with biotinylated secondary antibodies (1:200 dilution, Vector labs), followed by amplification using peroxidase-conjugated avidin (Vectastain Elite ABC kit, Vector labs) and treatment with 3,3'-diaminobenzadine substrate kit (Vector labs). All samples were counterstained with hematoxylin. Sections were imaged at the chiasm and proximal optic nerve, and photographed at 20x using a Nikon Eclipse E600 inverted microscope equipped with a Leica EC3 camera. All studies were performed in triplicate. Quantification was performed by

counting positive and negative cytosolic staining using the cell counting application in NIH ImageJ software. Cells were scored as immunopositive when antibody-mediated cytosolic staining was observed, while the total number of cells were identified by hematoxylin counterstaining. For each antibody, 3 randomly-selected images representing 3 individual mice per genotype (9 images total) were counted.

Quantitative real-time reverse transcribed RNA polymerase chain reaction (qRT-PCR).

qRT-PCR was performed using mouse *Mmp2*-specific primers (forward: 5'-CAGGGAATGAGTACTGGGTCTATT; reverse: 5'-ACTCCAGTTAAAGGCAGCATCTAC) on *Nf1*-deficient and wild-type (WT) astrocytes (n=3 independent samples each) generated and analyzed as previously described (6, 7).

Statistics

Statistics for AFM were performed using a custom MATLAB script, utilizing a two-way ANOVA test. Groups were considered to show a statistically significant difference for p-values < 0.05. Statistics for immunohistochemistry were performed using a student's t-test

Supplementary Figures

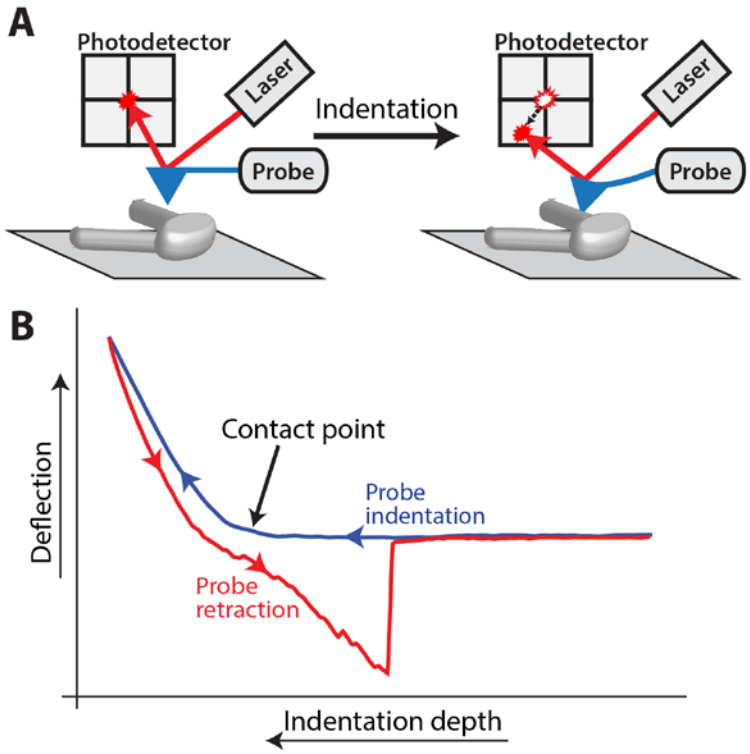

Figure S1. **Schematic depiction of AFM measurements in wild-type and *Nf1* glioma-bearing optic nerves**. **(A)** Graphic illustration of the methods used to obtain indentation curves by AFM. As the tip is lowered into the optic nerve sample, the spot where the laser strikes the photodetector changes, which is measured as a deflection. **(B)** Representative curves for probe indentation (blue) and retraction (red) on an optic nerve surface. Black arrow indicates the contact point for the probe.

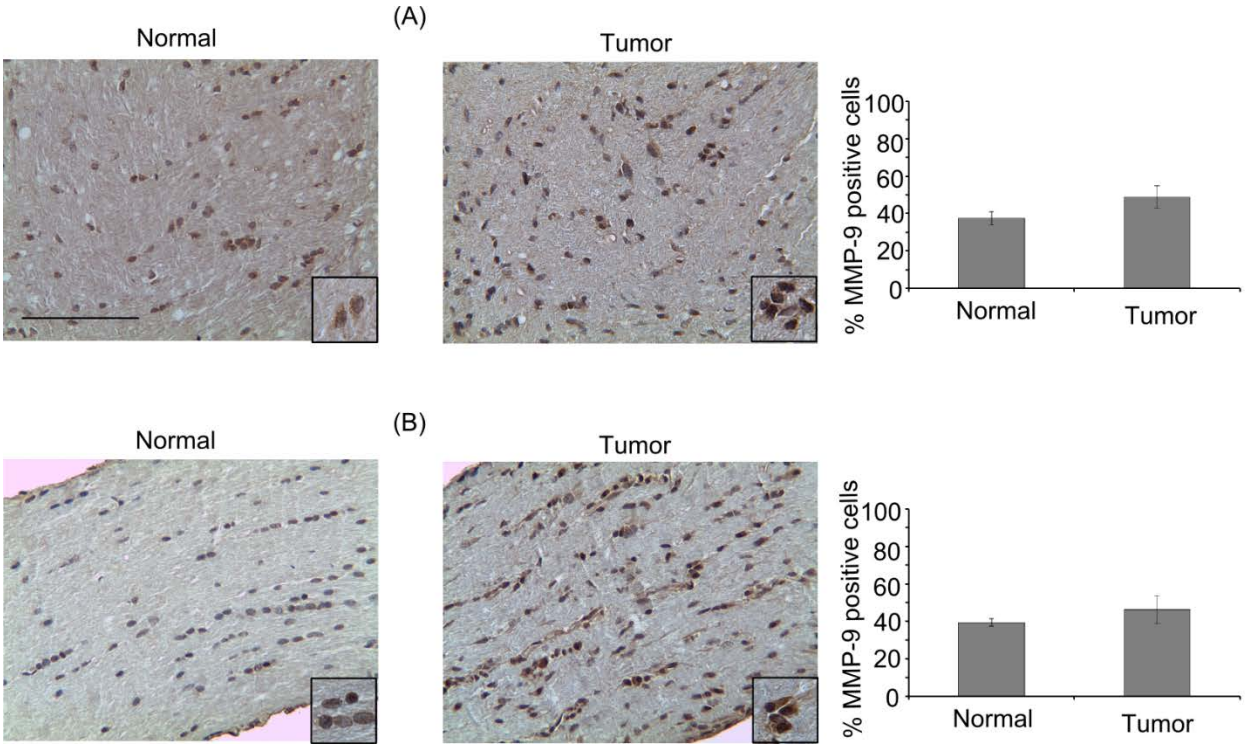

Figure S2. Glioma-bearing optic nerves show no change in MMP-9 expression relative to healthy optic nerves (normal) in both the chiasm (A) and optic nerve (B). Error bars represent SEM. Scale bar, 100 µm.

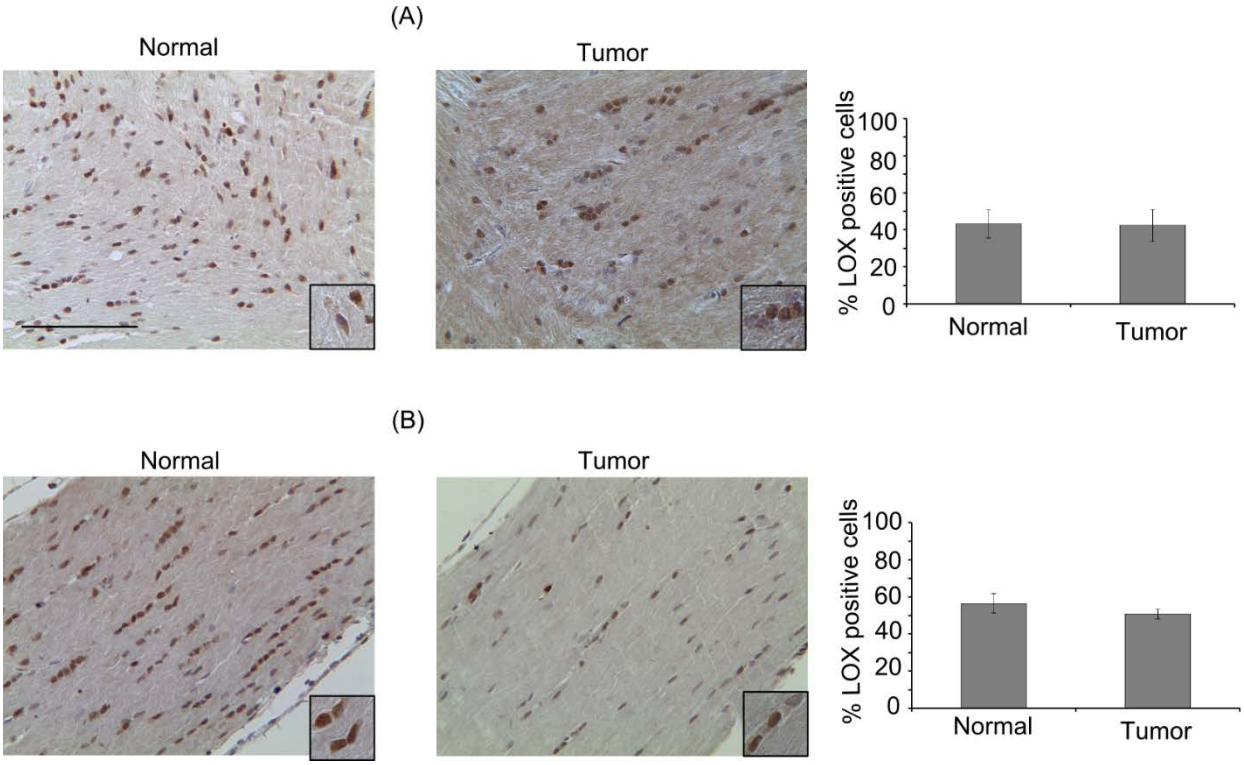

Figure S3. Glioma-bearing optic nerves show no change in LOX expression relative to healthy optic nerves (normal) in both the chiasm (A) and the optic nerve (B). Error bar represent SEM. Scale bar, 100 µm.

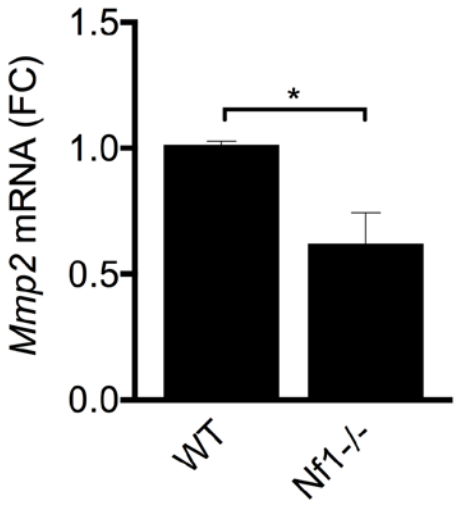

Figure S4. qRT-PCR analysis reveals a 40% decrease in *Mmp2* expression in *Nf1*-deficient astrocytes relative to their wild-type (WT) counterparts (n=3 samples each; p=0.033).

References

1. Toonen, J. A., Y. Ma, and D. H. Gutmann. 2016. Defining the temporal course of murine neurofibromatosis-1 optic gliomagenesis reveals a therapeutic window to attenuate retinal dysfunction. Neuro Oncol.
2. Bilodeau, G. G. 1992. Regular Pyramid Punch Problem. Journal of Applied Mechanics 59:519-523.
3. Li, Q. S., G. Y. H. Lee, C. N. Ong, and C. T. Lim. 2008. AFM indentation study of breast cancer cells. Biochemical and Biophysical Research Communications 374:609-613.
4. Mackay, J. L., and S. Kumar. 2013. Measuring the elastic properties of living cells with atomic force microscopy indentation. Methods Mol Biol 931:313-329.
5. Dimitriadis, E. K., F. Horkay, J. Maresca, B. Kachar, and R. S. Chadwick. 2002. Determination of elastic moduli of thin layers of soft material using the atomic force microscope. Biophysical journal 82:2798-2810.
6. Solga, A. C., W. W. Pong, K. Y. Kim, P. J. Cimino, J. A. Toonen, J. Walker, T. Wylie, V. Magrini, M. Griffith, O. L. Griffith, A. Ly, M. H. Ellisman, E. R. Mardis, and D. H. Gutmann. 2015. RNA Sequencing of Tumor-Associated Microglia Reveals Ccl5 as a Stromal Chemokine Critical for Neurofibromatosis-1 Glioma Growth. Neoplasia 17:776-788.
7. Smithson, L. J., and D. H. Gutmann. 2016. Proteomic analysis reveals GIT1 as a novel mTOR complex component critical for mediating astrocyte survival. Genes & Development 30:1383-1388.